doi: 10.2176/nmc.st.2020-0072

Neurol Med Chir (Tokyo) 60, 319–328, 2020

Online June 12, 2020

Hemodynamic and Histopathological Changes in the Early Phase of the Development of an Intracranial Aneurysm

Hiroharu KATAOKA,[1] Takanobu YAGI,[2] Taichi IKEDO,[1] Hirohiko IMAI,[3] Koichi KAWAMURA,[2] Kazumichi YOSHIDA,[1] Masanori NAKAMURA,[4] Tomohiro AOKI,[5] and Susumu MIYAMOTO[1]

[1]*Department of Neurosurgery, Kyoto University, Graduate School of Medicine, Kyoto, Kyoto, Japan*
[2]*Center for Advanced Biomedical Science, Waseda University, Tokyo, Japan*
[3]*Department of Systems Science, Graduate School of Informatics, Kyoto University, Kyoto, Kyoto, Japan*
[4]*Department of Mechanical Engineering, Nagoya Institute of Technology, Nagoya, Aichi, Japan*
[5]*Department of molecular pharmacology, National Cerebral and Cardiovascular Center, Suita, Osaka, Japan*

Abstract

Hemodynamic stress and chronic inflammation are closely associated with the pathogenesis of intracranial aneurysms (IAs). However, the hemodynamic and biological mechanisms triggering IA formation remain to be elucidated. To clarify them, computational fluid dynamics (CFD) and histopathological analyses in the early phase of IA development using an experimentally induced IA model in rats were conducted. Histological changes in the early phase of IA development were observed under a scanning electron microscope (SEM) and a transmission electron microscope (TEM). Using data from 7-T magnetic resonance angiography (7T-MRA), CFD analyses were performed to determine wall shear stress (WSS) and wall pressure (WP) at the prospective site of IA. A bump-like protrusion named an "intimal pad" was located in the anterior cerebral artery (ACA) immediately distal to the apex of the bifurcation. TEM showed the degeneration of the internal elastic lamina (IEL) and longitudinally elongated smooth muscle cells (SMCs) that switched from the contractile to the proliferative phenotype and penetrated between two divided layers of the degenerated IEL in the prospective site of the IA. However, no inflammatory cells were observed. CFD analyses showed no particular pattern of WSS and WP at the prospective IA site. IEL degeneration and the phenotypic change and longitudinal elongation of SMCs were identified as the early events in IA development. CFD analyses and TEM data suggest that these biological events may be derived from increased circumferential wall stress due to increased blood pressure and increased longitudinal wall strain due to the existence of the intimal pad.

Keywords: intracranial aneurysm, hemodynamics, internal elastic lamina, smooth muscle cell

Introduction

An intracranial aneurysm (IA) is an outward bulging of intracranial arteries and degenerative changes in the IA wall resulting in subarachnoid hemorrhage with high rates of morbidity and mortality. Recent advancements in molecular biology and engineering suggest that an IA develops due to disruption of a homeostatic balance in arterial walls induced by excessive hemodynamic stress.[1)] We established an experimentally induced rat IA model by loading hemodynamic stress to the rat intracranial artery[2)] and discovered a significant part of the molecular mechanisms involved in IA development.[3)] In this model, IA preferentially occurs at the bifurcation of the olfactory artery (OA) and the anterior cerebral

Received March 5, 2020; Accepted April 9, 2020

artery (ACA). It is assumed that abnormally high flow combined with defective crosslinking of collagen and elastin may induce IA formation at this site of the cerebral vasculature. However, we do not have the definite answer to the question why IA occurs preferentially at the OA-ACA bifurcation. It has also not been clarified which kinds of hemodynamic stress trigger IA formation. Moreover, the histopathological changes in the early phase of IA development in this model have not been investigated in detail.

Image-based computational fluid dynamics (CFD) analysis has been widely used in human IA studies.[4] Recently, we succeeded in the acquisition of vascular morphological data of the circle of Willis of rats using 7 Tesla-magnetic resonance imaging (7T-MRI).[5] Using the imaging data obtained by 7T-MRI and detailed vascular wall structure visualized under scanning electron microscope (SEM) examination, CFD analysis at the OA-ACA bifurcation in the rat IA model was performed to identify the hemodynamic factors inducing IA development. The histopathological changes in the early phase of IA development were observed using a transmission electron microscope (TEM) to clarify the key biological event triggering IA formation in response to the hemodynamic properties in the present study.

Materials and Methods

All animal experiments were conducted following the guidelines for Japan's Act on Welfare and Management of Animals. This study protocol was approved by the Institutional Animal Care and Use Committee and the Ethics Committee of Kyoto University.

IA induction in a rat model

Seven-week-old male Sprague Dawley rats were purchased from SLC (Shizuoka, Japan). IAs were induced as previously described.[2] Briefly, the left renal artery and the left common carotid artery (CCA) were ligated under general anesthesia induced with an intraperitoneal injection of 50 mg/kg pentobarbital (Kyoritsu Seiyaku, Tokyo, Japan). Animals were fed with chow containing 8% sodium chloride and 0.12% 3-aminopropionitrile (Tokyo Chemical Industry, Tokyo, Japan).

Electron microscopy

A total of 22 rats underwent electron microscopy. Rats were euthanized under general anesthesia before (n = 8), 1 day after (n = 6), or 3 days after (n = 8) IA induction. The circle of Willis of each rat was harvested and fixed in 3% glutaraldehyde solution (TAAB Laboratories Equipment, Aldermaston, UK) (pH 7.3) for 24 hours at room temperature for prefixation, followed by 2-hour immersion in 1% osmium acid solution (TAAB Laboratories Equipment) at room temperature for post-fixation. Samples for SEM were dehydrated through an ethanol series, critical point-dried, coated with evaporated gold-platinum, and observed (VE-9800, Keyence, Osaka Japan). Samples for TEM were dehydrated through an ethanol series, immersed into propylene oxide (Nisshin EM, Tokyo, Japan), and embedded into epoxy resin (TAAB Laboratories Equipment). Ultrathin-sliced samples were stained with 4.0% uranyl acetate (TAAB Laboratories Equipment) and 0.5% lead citrate (TAAB Laboratories Equipment) for routine examination and stained with 1.2% tannic acid (Nacalai Tesque, Kyoto, Japan), 5.0% uranyl acetate, and 0.1% lead citrate (TAAB Laboratories Equipment) for elastic fiber examination.[6] Stained samples were observed at 100 kV by TEM (H-7650, Hitachi-High-Tech, Tokyo, Japan).

Scoring of the internal elastic lamina at the OA-ACA bifurcation

Some animals were subjected to scoring of the internal elastic lamina (IEL) under TEM before IA induction (control), 1 day after IA induction (D1), or 3 days after IA induction (D3). The state of the IEL around the prospective site of the IA was classified into the following three categories: 0 = intact IEL; 1 = mildly degenerated IEL in which only the leading edge is fragmented; and 2 = severely degenerated IEL, divided into the two layers.

Computational fluid dynamics

A total of six control rats underwent 7T-MRI (BioSpec 70/20 USR, Bruker Biospin MRI, Ettlingen, Germany). Time-of-flight magnetic resonance angiography (MRA) was performed using a three-dimensional gradient echo with a flow compensation sequence. Spatial resolution was approximately $0.1 \times 0.1 \times 0.1$ mm^3. These images were imported to medical image visualization software (3D Slicer, ver.4.10.2, Brigham and Women's Hospital, Boston, MA, USA), with which three-dimensional surface meshes were produced. Due to the lack of spatial resolution, MRA failed to resolve the geometry of the intimal pad, which was instead measured by SEM (average height 30 μm) and added manually to the original geometry using modeling software (Rhinoceros 6, Robert McNeel & Associates, Seattle, WA, USA).

CFD analysis was carried out using commercial software (SCRYU/Tetra, Software Cradle, Newport

Beach, CA). An analyzed geometry was divided into several regions, followed by volume meshing (tetrahedron, prism), resulting in a total of 25-million meshes. The wall-nearest mesh was a few micrometers in height and was allocated into the surrounding region of the intimal pad. Three-dimensional, incompressible, and Newtonian modeling was accepted. The inlet and outlet boundary conditions were set by velocity, except the outlet of the OA where a constant pressure of 0 Pa was set. The ratio of the flow rate at a bifurcation (ICA-MCA, OA-ACA) was set to be a cubic ratio of the diameters of daughter vessels according to Murray's law.[7]

An inlet flow rate was estimated with uncertainty by referring to the available literature. Tohda showed that the mean flow rate of the CCA of SD rats (250–300 g) ranged from 2.5 to 3.0 mL/min.[8] García-Villalón measured the left CCA flow rate after right CCA ligation in Wistar rats (250–500 g), which increased from 3.4 to 4.2 mL/min (25% increase).[9] Taken together, the mean ICA flow rate after the ligation of the contralateral CCA was estimated to be in the order of 3.0 mL/min. In addition, the diastolic and systolic flow rates were estimated to be 1.5 and 6.0 mL/min, respectively. Several sets of flow rates were tested: (1) pulsatile flow (ICA flow rate of 1.5–6 mL/min); (2) steady flow (ICA flow rate of 1.5 and 6.0 mL/min); and (3) steady flow (ICA flow rate of 6.0 ml/min, and the OA-ACA flow rate ratio was changed to double the ACA flow rate compared to that of the benchmark; MCA flow rate unchanged).

In this model, aneurysmal changes are known to occur on the ACA at the region just distal to the intimal pad.[10] We set regions of interest (ROIs) in this site as the prospective site of the IA.

Statistical analysis

IEL scores are presented as medians (interquartile range). The Wilcoxon signed-rank test was used to compare two groups using SPSS software (version 20.0) (SPSS Japan, Tokyo, Japan). P <0.05 was considered significant.

Results

Electron microscopy of the OA-ACA bifurcation before IA induction

TEM imaging of the OA-ACA bifurcation before IA induction showed a three-dimensional ring-like protrusion at the beginning of the ACA entry, previously referred to as the intimal pad[11] (**Figs. 1A** and **1B**). An IA occurs preferentially immediately distal to the intimal pad at the apex.[11] The intimal pad was cross-sectionally asymmetric, like a right-angled triangle, with a sharp upslope in the OA side and a moderate downslope in the ACA side (**Figs. 1C** and **1D**). The average height of the intimal pad was in the order of 30 μm in a circumferential direction, and the height tended to increase toward the apex (**Fig. 1E**). Endothelial cells (ECs) aligned in parallel with the intimal pad on the OA side (**Fig. 1C**). In contrast, ECs on the ACA side aligned orthogonally with frequent overlapping (**Fig. 1D**). Smooth muscle cells (SMCs) in the media of the OA and ACA showed a contractile phenotype with abundant dense patches, focal densities, and filaments (**Fig. 1F**). These SMCs had round shapes, indicating that they were oriented in a circumferential direction. In contrast, SMCs in the intimal pad showed a synthetic phenotype with less dense patches, focal densities, and filaments and aligned dendritically at a connection between the intimal pad and the apex (**Fig. 1F**), where the IEL was disconnected (**Figs. 1G** and **1H**). In other sites, the IEL was preserved with a thickness of 2 μm, though the leading edge of the IEL was slightly fragmented in some cases (**Fig. 1H**).

Electron microscopy of the OA-ACA bifurcation after IA induction

TEM imaging of the OA-ACA bifurcation one day after IA induction showed that the leading edge of the IEL on the ACA side became thinner and fragmented, whereas that on the OA side was preserved (**Figs. 2A** and **2B**). As shown in **Fig. 2C**, the SMCs in the prospective site of the IA were elongated longitudinally along the ACA, with a needle-tip-like shape that appeared as if it would penetrate the leading edge of the IEL. The SMCs in this area showed a synthetic phenotype without abundant dense patches, focal densities, and filaments, whereas neighboring SMCs had a contractile phenotype (**Fig. 2B**). These SMCs were located together in a group in the area where the IEL was disrupted and appeared as if they would invade and destroy the IEL. The longitudinally elongated SMCs were only observed on the ACA side, and the number of these SMCs increased 1 day after IA induction (**Fig. 2B**).

SMCs at the intimal pad had a synthetic phenotype and were aligned in parallel with the intimal pad (**Fig. 2D**). SMCs on the contralateral side shared similarities with those in the apex, including a longitudinally elongated shape, a synthetic phenotype, and an IEL-invading appearance, which were enclosed by circumferentially oriented contractile SMCs. However, IEL continuity was still preserved, though it became thinner and slightly fragmented (**Fig. 2E**).

No inflammatory cells including macrophages were observed at the OA-ACA bifurcation 1 day and 3 days after IA induction.

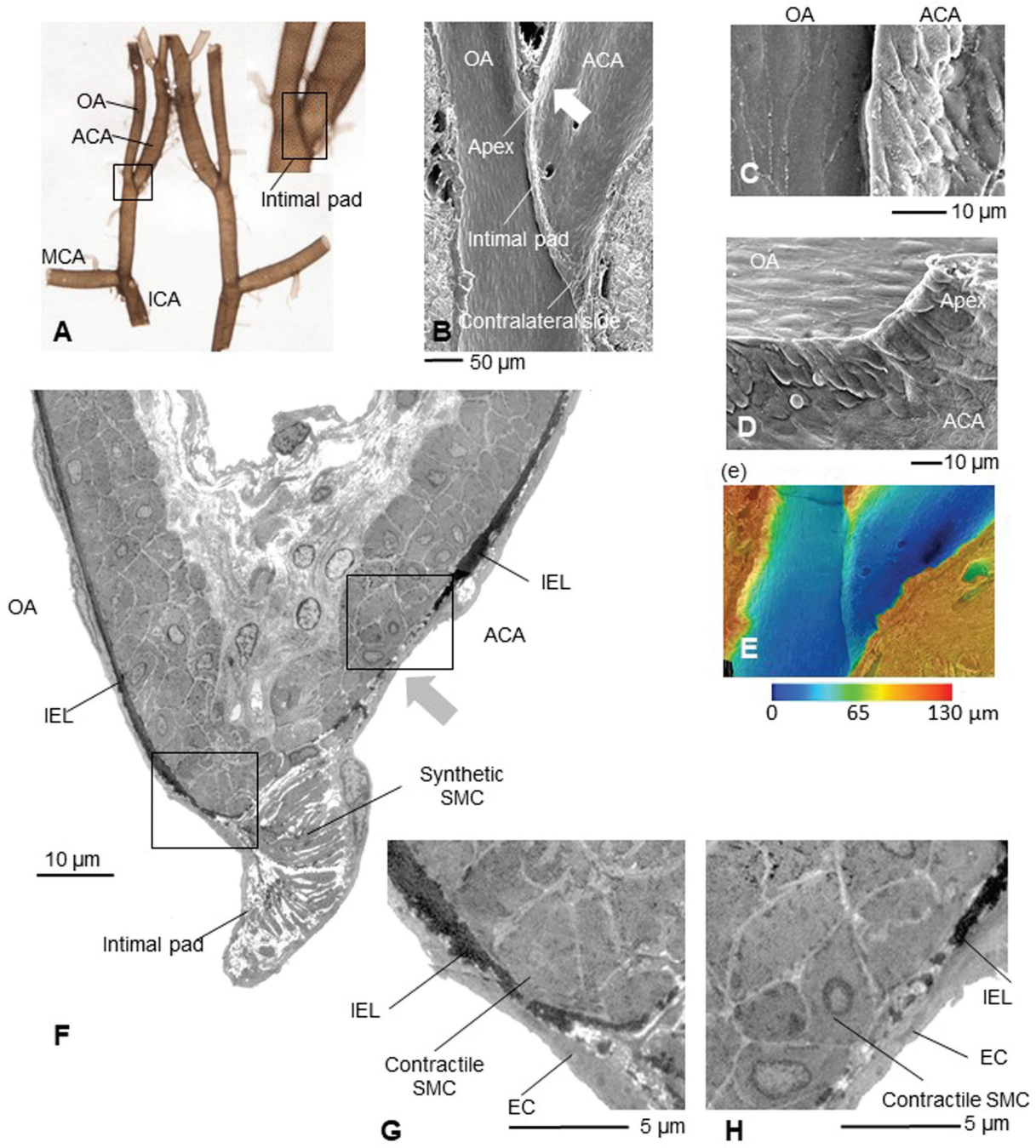

Fig. 1 Electron microscopy imaging of the OA-ACA bifurcation before IA induction. (A) The circle of Willis in a rat observed under a stereomicroscope. (B) SEM imaging of the intimal surface at the OA-ACA bifurcation. The white arrow indicates the prospective site of the IA. Bar = 50 μm (C and D) Magnified images of the intimal pad. Bar = 10 μm (E) Measurement of the height of the intimal pad by SEM. (F) TEM imaging of the overview of the OA-ACA bifurcation. The gray arrow indicates the prospective site of the IA. (G and H) Magnified views at the leading edge of the internal elastic lamella (green-painted) at the OA (G) and the ACA (H). Bar = 5 μm. ACA: anterior cerebral artery, IA: intracranial aneurysm, ICA: internal carotid artery, IEL: internal elastic lamina, MCA: middle cerebral artery, OA: olfactory artery, SEM: scanning electron microscopy, TEM: transmission electron microscopy.

IEL scoring at the OA-ACA bifurcation

Of 22 rats undergoing TEM, 15 (control: 4, D1: 5, D3: 6) were subjected to scoring of the IEL. As shown in **Fig. 3**, the IEL score was significantly higher on the ACA side (D1: 2 [IQR, 1–2]; D3: 1.5 [IQR, 1–1.875]) than on the OA side (D1: 0 [IQR,

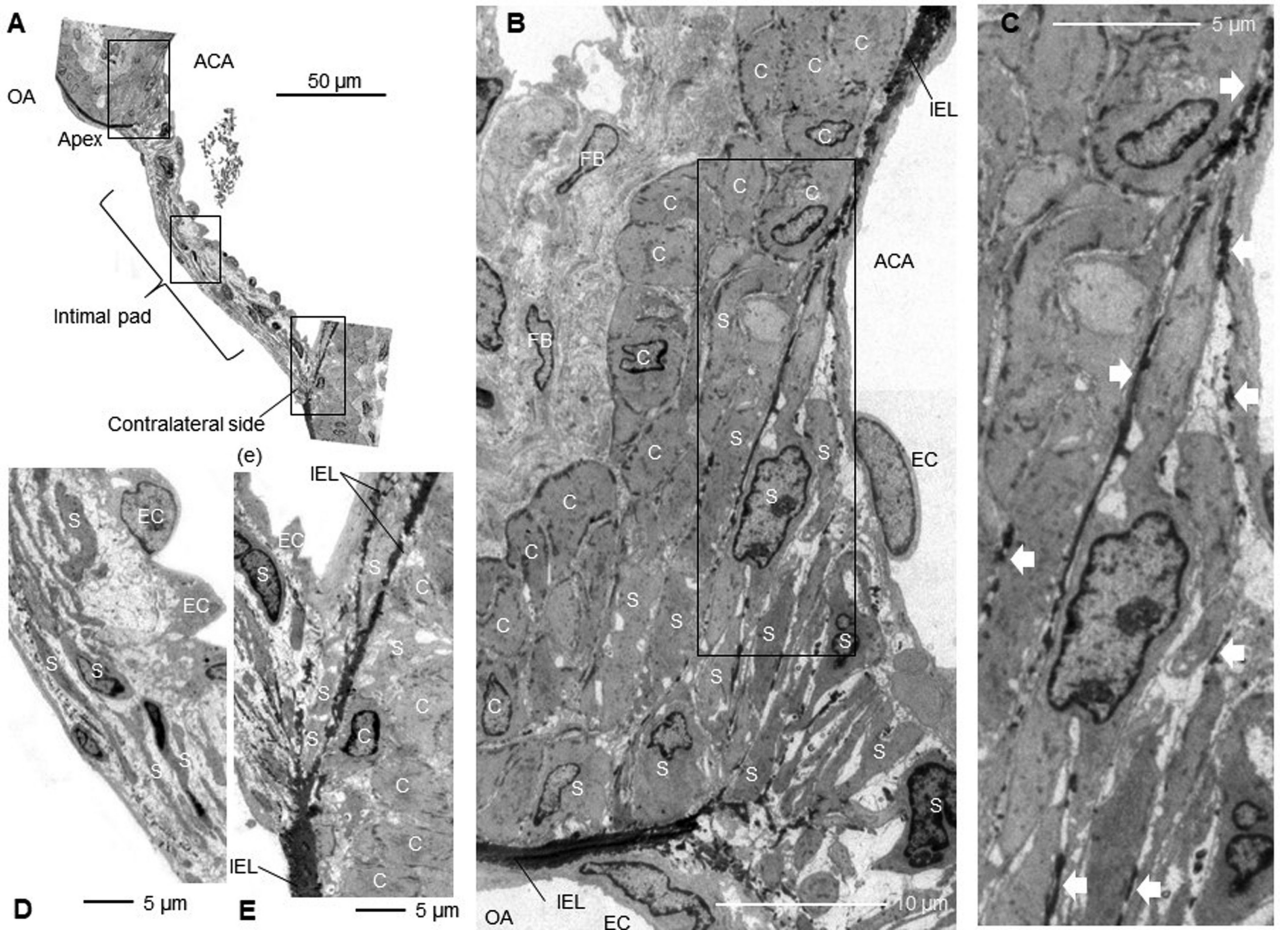

Fig. 2 Transmission electron microscopy imaging of the OA-ACA bifurcation one day after IA induction. (A) An overview of the OA-ACA bifurcation. Bar = 50 μm (B) Magnified image of the apex. On the ACA side. C and S denote contractile and synthetic smooth muscle cells, respectively. Bar = 10 μm (C) A more magnified image at the leading edge of the IEL on the ACA side. White arrows indicate the fragmented and thinning IEL. Bar = 5 μm (D and E) A magnified image of the intimal pad (D) and the contralateral side (E). Bar = 5 μm. ACA: anterior cerebral artery, EC: endothelial cell, FB: fibroblast, IA: intracranial aneurysm, IEL: internal elastic lamina, OA: olfactory artery.

0–0]; D3: 0 [IQR, 0–0]), both 1 day (P = 0.041) and 3 days (P = 0.019) after IA induction, whereas the IEL score was not different between the OA side (0 (IQR, 0–0)) and the ACA side (0 (IQR, 0–0)) before IA induction (P = 1.00). These data indicate that IEL degeneration occurs immediately after IA induction on the ACA side.

Computational fluid dynamics

Figure 4 shows the wall shear stress (WSS) and wall pressure (WP) contours at the OA-ACA bifurcation. It was assumed that the vascular geometry as early as 1–3 days after IA induction remained unchanged compared to that before IA induction. No subject-specific flow rate information was available. Thus, as described in Materials and Methods, several sets of inflow rates and outflow rate ratios, including steady-flow and pulsatile-flow conditions, were compared. There were no noteworthy differences in WSS and WP among these boundary conditions, as well as among the six rats tested (data not shown). Therefore, a representative case, which was obtained in a steady-flow condition with an ICA flow rate of 6.0 mL/min and benchmark outlet flow conditions as detailed in Materials and Methods, is presented.

In all the six cases, WSS was concentrated on the OA side at the OA-ACA bifurcation, where IAs never develop (**Fig. 4B**). At the prospective site of IA, the WSS failed to show a notable pattern, though there was a slight increase in WSS at a neighboring site. However, the increase was negligible compared to that on the OA side. Owing to the Y-shaped geometry of bifurcation, the WP at the apex was

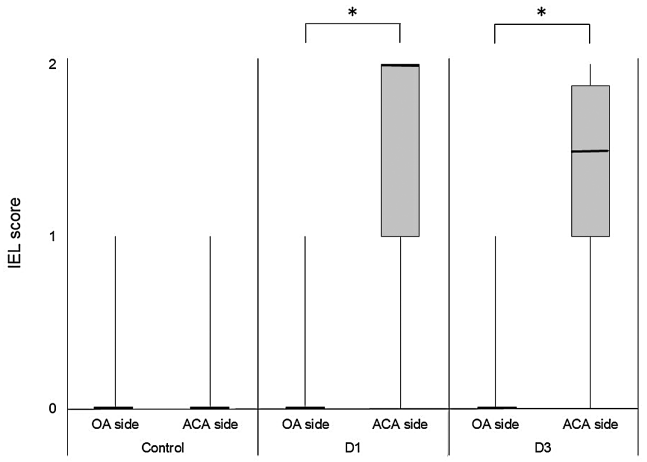

Fig. 3 Comparison of the IEL scores on the OA side and the ACA side. The state of the IEL before IA induction (control; n = 4), 1 day after IA induction (D1; n = 5), and 3 days after IA induction (D3; n = 6) was scored using the following three grades under TEM: 0 = intact IEL; 1 = mildly degenerated IEL in which only the leading edge is fragmented; and 2 = severely degenerated IEL, divided into the two layers. The IEL score is expressed in a box plot and compared between the OA side and the ACA side by the Wilcoxon signed-rank test. * P < 0.05. ACA: anterior cerebral artery, IA: intracranial aneurysm, IEL: internal elastic lamina, OA: olfactory artery, TEM: transmission electron microscopy.

concentrated, and the presence of the intimal pad produced an asymmetric pattern. Thus, high WP was observed between the apex and the junction of the intimal pad where IA never develops.

Discussion

Degeneration of the IEL is a hallmark of early aneurysmal change.[12] However, when it appears, what triggers it, and how it progresses remain inconclusive. To the best of our knowledge, this is the first study focusing on the early events in IA development by combining electron microscopy and CFD analyses. It was found that IEL degeneration occurred immediately after IA induction at the prospective site of the IA, which is in line with the findings reported recently by Koseki et al.[13] In addition, the transformation of contractile SMCs to the synthetic phenotype occurred at the same site. The phenotypic modulation of SMCs was found in the IA wall, especially in the neck region.[14] This is the first report showing that the SMC transformation occurs in the early phase in IA development. It is noteworthy that the IEL degeneration and the phenotypic change in SMCs appeared only on the ACA side. The synthetic SMCs were elongated longitudinally, exhibited a

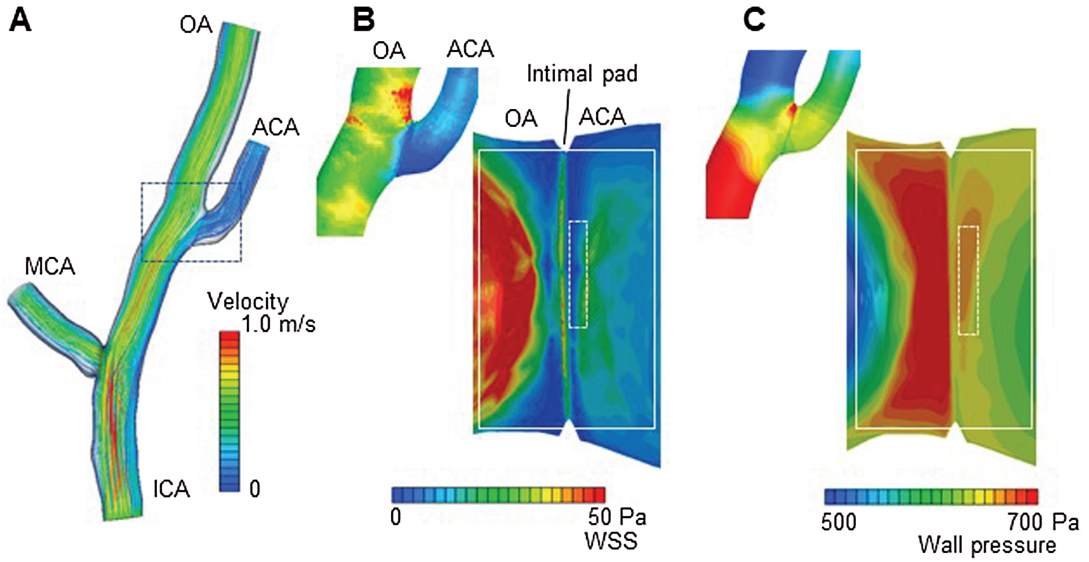

Fig. 4 Hemodynamics of the OA-ACA bifurcation by computational fluid dynamics analysis. (A) Streamlines with velocity magnitude, (B) WSS, and (C) WP. WSS and WP are also zoomed from the top view, where the white dotted-line area corresponds to the site of the prospective site of the IA, and the white solid-line area corresponds to the OA and ACA origin at the apex. Note that the WP is defined as a differential pressure between the inlet and outlet arteries due to the principles of CFD. For the actual pressure, blood pressure should be added. ACA: anterior cerebral artery, CFD: computational fluid dynamics, ICA: internal carotid artery, MCA: middle cerebral artery, OA = olfactory artery, WP: wall pressure, WSS: wall shear stress.

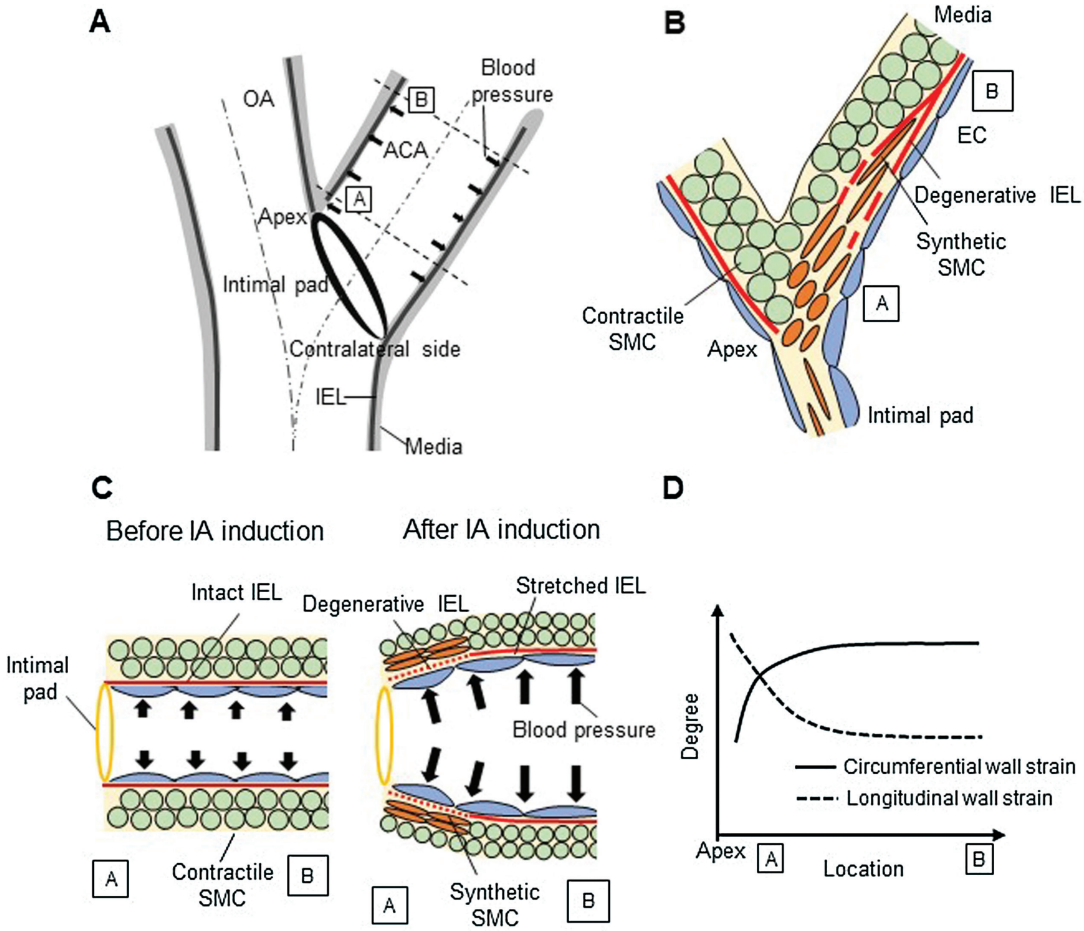

Fig. 5 Schematic drawings explaining the mechanisms of the early events of experimentally induced IA development at the OA-ACA bifurcation in rats. (A) A schema of the anatomical structure in the OA-ACA bifurcation. The intimal pad is located in the ACA origin. The IEL at the apex on the ACA side is inherently disrupted. Squares A and B denote the proximal and distal edges of the prospective site of the IA, respectively. (B) A schema of the apex of the OA-ACA bifurcation after IA induction. The IEL in this site is fragmented and divided into two layers from the leading edge of the ACA side. SMCs at this site switch the phenotype to the synthetic type and are elongated longitudinally. These synthetic SMCs penetrate between the two layers of the degenerative IEL. (C) A simplified model showing the mechanobiological responses in the prospective site of the IA. An elevated blood pressure after IA induction results in increased circumferential wall stress in the whole artery. The intimal pad serves as a mechanical constraint for dilation and circumferential wall strain at the site adjacent to the intimal pad, resulting in increased longitudinal wall strain at this site. The increased longitudinal wall strain is assumed to cause the phenotypic change and longitudinal elongation of SMCs. (D) The estimated relationship between the circumferential and longitudinal wall strains in the vascular wall at the prospective site of the IA after abrupt blood pressure elevation. The existence of the intimal pad restricts the circumferential wall strain at the site adjacent to the intimal pad. Consequently, the longitudinal wall strain increases at this site. ACA: anterior cerebral artery, IA: intracranial aneurysm, IEL: internal elastic lamina, OA: olfactory artery, SMCs: smooth muscle cells.

needle-tip-like shape, which appeared as if it would penetrate and invade the leading edge of the IEL. Interestingly, the invading SMCs migrated together in a group beyond the IEL to the intima and seemed to facilitate IEL degeneration and inhibit its repair. These SMCs prevailed at the apex toward the leading edge of the IEL in the ACA (**Fig. 5B**).

Previous CFD analyses of human IAs[15] and IAs induced in a rabbit model[16] have implicated high WSS as a trigger of IA formation. However, the results of the present CFD analysis demonstrated that WSS at the prospective site of the IA in this model was not higher than at other sites. Although WP at the apex of the OA-ACA bifurcation was slightly higher

by about 200 Pa than that in a neighboring area, the maximum WP was applied to the vessel wall proximal to the intimal pad, where IA never develops. According to the previous report,[13] blood pressure increases from 130 mmHg to 170 mmHg on day 1 after IA induction in this model. Given that 40 mmHg corresponds to 5333 Pa, the amount of the pressure difference caused by blood flow would be negligible compared to that caused by the increase in blood pressure. Therefore, we cannot explain why IA occurs exclusively in the OA-ACA bifurcation by forces, such as WSS and WP, applied to the surface of the vascular wall by blood flow. Instead, the findings in the present study led us to the idea that the early events in IA development may be derived from vascular wall stress and strain. On the other hand, Nakatani et al. reported that WSS was highest at the distal end of fully developed IA orifice in this model, suggesting that WSS may has an influence on IA enlargement.[10]

Vascular wall stress is a force acting on a unit area inside a blood vessel. On the other hand, vascular wall strain is defined as the mechanical deformation of the vascular wall in response to applied forces. Because the circumferential wall stress is proportional to blood pressure,[17] it increases abruptly immediately after IA induction. In addition, the intimal pad has a ring-like structure on the luminal surface of the vascular wall, serving as a mechanical constraint for the circumferential strain at the area adjacent to the intimal pad (**Fig. 5C**). SMCs in the intimal pad were stretched circumferentially even in a physiological condition, supporting this notion. Then, the restricted circumferential wall strain due to the intimal pad increased the longitudinal wall strain in response to increased blood pressure at this site (**Figs. 5C** and **5D**). Thus, the prospective site of the IA suffers from increased circumferential wall stress and increased longitudinal wall strain, making SMCs oriented and elongated in a longitudinal direction. Indeed, real-time imaging showed outward stretched wall motions at this site.[18] Physiological stress promotes the contractile SMC phenotype, whereas over- or under-stressing provokes modulation toward the synthetic phenotype.[19] The present results suggest that these mechanical factors may modulate the SMC phenotype. Although endothelium-mediated shear stress may also have an effect on the phenotypic change of SMCs, the effect is assumed to be small because WSS at the prospective site of the IA showed no notable pattern.

Previous studies have identified the essential role of macrophage-mediated inflammation in IA development.[20,21] The number of macrophages infiltrated in the IA wall increased with IA development.[22] Pharmacological depletion of macrophages dramatically inhibited IA formation.[23] However, there were no macrophages in the prospective site of the IA until 3 days after IA induction, which is compatible with the findings reported by Koseki et al.[13] They observed transendothelial migration of macrophages 5 days after IA induction, suggesting that the IEL disruption precedes macrophage accumulation.

Taken together, the IEL degeneration and the phenotypic transformation of SMCs were identified as the early key events in IA development. It was assumed that these biological events might result from the increased circumferential wall stress resulting from increased blood pressure and the longitudinal wall strain due to the constraint by the intimal pad, rather than from high WSS. Interestingly, this series of phenomena was also observed at the contralateral side in the ACA origin to a modest degree, further supporting our assumption. The difference between the apical side and the contralateral side may be derived from the fact that the IEL at the apex has an inherent discontinuity in physiological state.

This study has potential limitations. First, this was an experimental study using an animal model. Whether the same events occur in the early stage of human IAs has not been confirmed. However, it is highly possible that similar mechanisms are involved in the formation of human IAs considering the facts described below. The IEL at the apices of bifurcations sometimes showed fragmentation and degradation.[24] Sato et al. observed IEL defects in the vertebral artery near the origin of the posterior inferior cerebellar artery, where saccular IAs and arterial dissection arise frequently.[24] Thus, an innate or acquired fragility of the IEL is likely to be involved in the genesis of human IAs. Intimal pads were observed at and distal to the carinas of bifurcations in human postmortem intracranial arteries.[25] Moreover, intimal pads covered a much wider area of vessel wall proximal to the necks of IAs,[25] supporting our notion that the intimal pad has a crucial role in IA formation. Second, mechanisms of IEL degeneration remain to be clarified. One can presume that synthetic SMCs or activated endothelium might produce some kinds of protease. MMP-2 and -9 were preferentially expressed in SMCs adjacent to the damaged IEL in a rabbit model.[26] Although this finding has not been confirmed in the rat OA-ACA model, MMP expression in transformed SMCs might be a cause of IEL degeneration.

Despite the above-mentioned limitations, the present findings provide a better understanding of the early stage of IA development. There is no doubt that an IA develops as a result of pathological remodeling of the vascular wall. Hemodynamic stress and biological responses leading to wall degeneration are two major factors facilitating the disease process of IA. Our approach combining molecular biology and engineering will shed light on the mechanobiological coupling involved in IA development.

Acknowledgments

This work was supported in part by grants from the Japan Society for the Promotion of Science JSPS KAKENHI: Grants No. 15H04952.

Conflicts of Interest Disclosure

The authors have no personal financial or institutional interest in any of the drugs, materials, or devices in the article. H.K., T.I., K.Y., and S.M are members of The Japan Neurosurgical Society (JNS) and have registered online Self-reported COI Disclosure Statement Forms through the website for JNS members.

References

1) Frosen J, Cebral J, Robertson AM, Aoki T: Flow-induced, inflammation-mediated arterial wall remodeling in the formation and progression of intracranial aneurysms. *Neurosurg Focus* 47: E21, 2019
2) Hashimoto N: Experimental model for producing cerebral aneurysms. *J Neurosurg* 66: 634–635, 1987
3) Kataoka H: Molecular mechanisms of the formation and progression of intracranial aneurysms. *Neurol Med Chir (Tokyo)* 55: 214–229, 2015
4) Xiang J, Tutino VM, Snyder KV, Meng H: CFD: computational fluid dynamics or confounding factor dissemination? The role of hemodynamics in intracranial aneurysm rupture risk assessment. *AJNR Am J Neuroradiol* 35: 1849–1857, 2014
5) Ikedo T, Kataoka H, Minami M, et al.: Sequential inward bending of arterial bifurcations is associated with intracranial aneurysm formation. *World Neurosurg* 129: e361–e366, 2019
6) Kajikawa K, Yamaguchi T, Katsuda S, Miwa A: An improved electron stain for elastic fibers using tannic acid. *J Electron Microsc (Tokyo)* 24: 287–289, 1975
7) Murray CD: The physiological principle of minimum work: I. The vascular system and the cost of blood volume. *Proc Natl Acad Sci USA* 12: 207–214, 1926
8) Tohda K, Masuda H, Kawamura K, Shozawa T: Difference in dilatation between endothelium-preserved and -desquamated segments in the flow-loaded rat common carotid artery. *Arterioscler Thromb* 12: 519–528, 1992
9) García-Villalón AL, Roda JM, Alvarez F, Gómez B, Diéguez G: Carotid blood flow in anesthetized rats: effects of carotid ligation and anastomosis. *Microsurgery* 13: 258–261, 1992
10) Nakatani H, Hashimoto N, Kang Y, et al.: Cerebral blood flow patterns at major vessel bifurcations and aneurysms in rats. *J Neurosurg* 74: 258–262, 1991
11) Kojima M, Handa H, Hashimoto N, Kim C, Hazama F: Early changes of experimentally induced cerebral aneurysms in rats: scanning electron microscopic study. *Stroke* 17: 835–841, 1986
12) Hazama F, Hashimoto N: An animal model of cerebral aneurysms. *Neuropathol Appl Neurobiol* 13: 77–90, 1987
13) Koseki H, Miyata H, Shimo S, et al.: Two diverse hemodynamic forces, a mechanical stretch and a high wall shear stress, determine intracranial aneurysm formation. *Transl Stroke Res* 11: 80–92, 2020
14) Nakajima N, Nagahiro S, Sano T, Satomi J, Satoh K: Phenotypic modulation of smooth muscle cells in human cerebral aneurysmal walls. *Acta Neuropathol* 100: 475–480, 2000
15) Kulcsár Z, Ugron A, Marosfoi M, Berentei Z, Paál G, Szikora I: Hemodynamics of cerebral aneurysm initiation: the role of wall shear stress and spatial wall shear stress gradient. *AJNR Am J Neuroradiol* 32: 587–594, 2011
16) Meng H, Wang Z, Hoi Y, et al.: Complex hemodynamics at the apex of an arterial bifurcation induces vascular remodeling resembling cerebral aneurysm initiation. *Stroke* 38: 1924–1931, 2007
17) Humphrey JD: Mechanisms of arterial remodeling in hypertension: coupled roles of wall shear and intramural stress. *Hypertension* 52: 195–200, 2008
18) Miyata H, Shimizu K, Koseki H, et al.: Real-time imaging of an experimental intracranial aneurysm in rats. *Neurol Med Chir (Tokyo)* 59: 19–26, 2019
19) Rensen SS, Doevendans PA, van Eys GJ: Regulation and characteristics of vascular smooth muscle cell phenotypic diversity. *Neth Heart J* 15: 100–108, 2007
20) Aoki T, Kataoka H, Ishibashi R, Nozaki K, Egashira K, Hashimoto N: Impact of monocyte chemoattractant protein-1 deficiency on cerebral aneurysm formation. *Stroke* 40: 942–951, 2009
21) Aoki T, Nishimura M, Matsuoka T, et al.: PGE(2) -EP(2) signalling in endothelium is activated by haemodynamic stress and induces cerebral aneurysm through an amplifying loop via NF-κB. *Br J Pharmacol* 163: 1237–1249, 2011
22) Aoki T, Kataoka H, Morimoto M, Nozaki K, Hashimoto N: Macrophage-derived matrix metalloproteinase-2 and -9 promote the progression of cerebral aneurysms in rats. *Stroke* 38: 162–169, 2007
23) Kanematsu Y, Kanematsu M, Kurihara C, et al.: Critical roles of macrophages in the formation of intracranial aneurysm. *Stroke* 42: 173–178, 2011

24) Suzuki K, Hori S, Ooneda G: Electron microscopic study on the medial defect at the apex of human cerebral arterial bifurcations. *Virchows Arch A Pathol Anat Histol* 382: 151–161, 1979
25) Sheffield EA, Weller RO: Age changes at cerebral artery bifurcations and the pathogenesis of berry aneurysms. *J Neurol Sci* 46: 341–352, 1980
26) Kolega J, Gao L, Mandelbaum M, et al.: Cellular and molecular responses of the basilar terminus to hemodynamics during intracranial aneurysm initiation in a rabbit model. *J Vasc Res* 48: 429–442, 2011

Address reprint requests to: Hiroharu Kataoka, MD, PhD, 54 Shogoinkawahara-cho, Sakyo-ku, Kyoto, Kyoto 606-8507, Japan
e-mail: kataoka@kuhp.kyoto-u.ac.jp